

Alternate block shear in beams: Experimental and FE fracture modeling

Mazen B. Helwe, Sana N. El Kalash, Elie G. Hantouche*

Department of Civil and Environmental Engineering, American University of Beirut, Lebanon



ARTICLE INFO

Keywords:

Alternate block shear
Experiment
Steel beam
Fracture
Strength model

ABSTRACT

This study investigates experimentally and analytically the alternate block shear (ABS) failure in steel beams. ABS might be a potential failure mode of beams in bolted connections subjected to pure tensile forces. The results of a series of four specimens are presented and discussed. The experimental results showed that the ABS failure path is a combination of both yielding and rupture mechanisms leading to a ductile failure in the beam. Also, the experimental results showed that as the connection length decreases and/or beam depth increases the ABS failure mode governs. The experimental results indicate that the ABS failure have a lower capacity than the classical block shear failure and is a ductile failure mode. Thus, post-yielding strength and ductility are needed to be predicted using finite element (FE) fracture modeling. FE fracture simulations, including tensile and shear fracture modeling, are developed to predict the experimental results after first component failure. The *Rice and Tracey* and the *Hooputra* models are associated with all steel materials to model their ductile damage under tensile and shear loading, respectively. Prior to experimental validation, both base and bolt materials are calibrated for stress-strain and stress triaxiality-strain at fracture responses. The results showed that the FE fracture models can predict with acceptable accuracy the experimental results of force-deformation and the behavior and failure path of the tested specimens. The objective of this study is to expand the experimental and numerical database in investigating the ABS failure mode. This study will guide designers to include ABS in the current design procedures as a limit state.

1. Introduction

Steel connections are commonly designed by considering a range of potential failure modes, assessing the capacity for each mode, and taking the lowest mode as the governing for the connection. All other potential failure modes are then compared to the lowest mode and arranged from the lowest to the highest to obtain the sequence of potential failures.

Typical failure modes of beams in steel connections include plastic hinging (gross section yielding), net section fracture (NSF), block shear, and bolt tear-out and bearing. However, there are potential failure modes that might occur besides the aforementioned ones. The atypical failure mode in Tees connected through their flange was reported in the literature and termed as alternate block shear (ABS). This failure mode is similar to the traditional block shear failure mode which is recognized as a limit state in beams of moment connections as per the ANSI/AISC 358-16 [1]. The failure mechanism of block shear combines a tensile fracture in one plane and shear failure (yielding or rupture) in the transverse plane. The ABS is defined as a combination of full tensile fracture in the beam flange followed by an alternate shear failure path

propagating in the beam web toward the edge. Fig. 1 shows the block shear and ABS failures in a beam section connected to a flange plate. The block shear failure is considered a ductile failure mode and is available in the ANSI/AISC 360-16 specifications [2], unlike the ABS failure which is not recognized as a limit state.

ABS might be a potential failure mode of beams in bolted connections subjected to pure tensile forces. However, current design codes do not include the ABS failure mode check. Considering the general case of I beam sections, block shear failure consists of two shear planes in the beam flange (Fig. 1(a)) while ABS failure consists of one shear plane in the beam web (Fig. 1(b)). Knowing that the beam web thickness is usually smaller than the beam flange thickness, ABS failure might have a lower capacity than the block shear failure. Therefore, it is essential to investigate experimentally and analytically the ABS failure in steel beams. Also, it is important to include ABS failure check in the available design codes to ensure a safe design.

Existing experimental and analytical research dealt with structural Tee connections to investigate the ABS failure. Epstein [3] and Epstein and McGinnis [4] investigated the ABS phenomenon as a governing failure mode in structural Tee connections. Also, Epstein and Stamberg

* Corresponding author at: Department of Civil and Environmental Engineering, American University of Beirut, P.O. Box 11-0236, Riad El-Solh/Beirut 1107 2020, Lebanon.

E-mail addresses: mbh16@mail.aub.edu (M.B. Helwe), sne08@mail.aub.edu (S.N. El Kalash), eh12@aub.edu.lb (E.G. Hantouche).

<https://doi.org/10.1016/j.engstruct.2019.02.014>

Received 31 July 2018; Received in revised form 26 December 2018; Accepted 5 February 2019

Available online 15 February 2019

0141-0296/© 2019 Elsevier Ltd. All rights reserved.

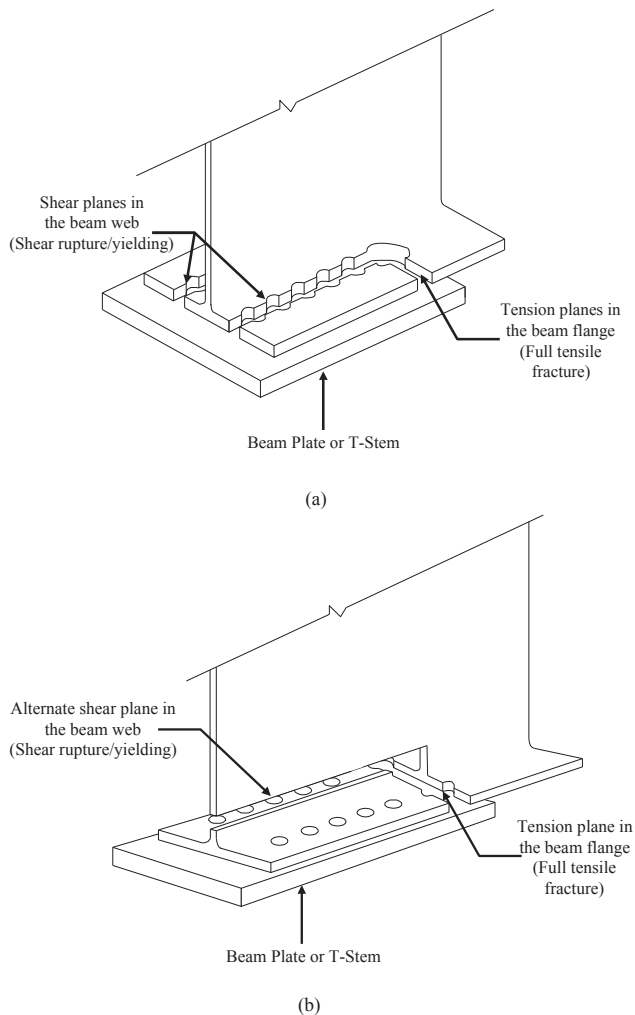


Fig. 1. (a) Typical block shear failure path and (b) alternate block shear failure path in W beam section connected to thick plate.

[5] reported the experimental results of structural Tee connections by varying the connection length, beam depth, and eccentricity. The results showed that as the connection length decreases or beam depth increases, the failure mode is controlled by ABS. Moreover, Epstein [3] provided a strength model that is capable of predicting the ABS capacity. Also, Driver et al. [6] and Cai and Driver [7] proposed a *unified* strength model that is capable to predict both ABS and block shear failure load capacities. The *unified* strength model takes into consideration that shear failure is a combination of ultimate and yield stresses and is considered a ductile mechanism.

Despite the experimental and analytical research performed on ABS failure in Tee connections, additional research work needs to be conducted to investigate the ABS failure in beams of steel connections. Moreover, ABS is considered a ductile failure mode and can potentially happen after beam plastic hinging. Therefore, it is essential to study analytically the pre and post-yielding responses of beams failing in ABS.

All existing FE analyses, found in the literature, model the behavior of steel connections until first component yielding. However, FE fracture modeling is required for the analytical investigation to model the response after first component yielding. In fact, ductile fracture of steel starts from inherent flaws, present in the material, that grow into micro voids due to strain and stress demands. In this research, the ductile fracture due to both tension and shear stresses in the ABS failure mode is modeled.

The aim of this research is to investigate experimentally and analytically the ABS failure in beams of steel connections when subjected to

monotonic tensile loading. For this purpose, four tests varying the beam depth and the connection length (by varying the number of shear bolts), are performed. In addition, existing strength models available in the literature are tested against the experimental results conducted in this study to demonstrate their prediction capabilities. Also, a comparison is made between the ABS and the block shear capacities of the tested specimens to prove that ABS is more critical than block shear. Then, FE fracture models are developed to validate the experimental results before and after first component yielding. This will provide additional dataset to simulate the behavior of ABS in steel connections in future parametric studies. The results of this research will expand the experimental and analytical database of investigating the ABS failure mode. This aims at including the ABS failure as a limit state in the current steel design codes to ensure a safe design.

2. Experimental program and test results

In order to investigate the strength and behavior of ABS failure mode in beams of steel connections, a number of experimental tests were carried out as part of this research. Test specimens were designed to examine the effects of two parameters (connection length and beam depth) on the ABS failure mode and connection strength. The objectives of this experimental program are to: (1) expand the pool of available experimental data, (2) assess the ability of the existing strength models to predict the capacity of ABS in beams of steel connections, (3) provide data to develop and calibrate FE fracture models describing the behavior of ABS.

To fulfill the above mentioned objectives, four component tests of thick plate connected to beam section were tested under monotonic loading. While ABS is likely to occur in any W, M, S, HP, WT, MT, ST, or built-up I section, the focus of this research is on I sections (equivalent of the IPE sections in the Eurocode3). The beam sections used in the experiment are: IPE 220 (two specimens), IPE 240 (one specimen), and IPE 270 (one specimen). The experimental results conducted in this study can be used as a benchmark for future experimental tests on full scale connections.

2.1. Geometry of specimens and material properties

The beam depth and number of shear bolts were varied to identify the geometric parameters that affect the ABS failure mode. These parameters were reported in the literature to impact the ABS failure mode. Details of the main geometric and material characteristics of the specimens are presented in Fig. 2 and Table 1. For specimens MC1, MC2, and MC3 having the same number of shear bolts (3 bolts per row), the beam depth was varied using different beam sections (IPE 220, IPE 240, and IPE 270, respectively). For specimen MC4 having the same beam section as MC1, the number of shear bolts was increased to 4 bolts per row. The flange plate thickness used was 25 mm (1 in.).

The component beams were connected to thick plates (S355) using M18 and M20 (grade 10.9) shear bolts. For all specimens, MC4, taken as a reference specimen, was designed to fail by NSF in the beam and MC1, MC2, and MC3 were designed to fail by ABS in the beam.

2.2. Experimental setup, test arrangement, and loading conditions

An overall view of the test set-up and a schematic drawing of the test assembly configuration are shown in Fig. 3. Six linear variable differential transformers (LVDTs) were used to record the beam deformation throughout the test. LVDTs 1 and 2 were installed to record any deformation at the restrained surface of the specimen, and LVDTs 3, 4, 5, and 6 were installed to record the deformation of the specimen as shown in Fig. 4. The total displacement in the beam was computed as the deduction of the average of LVDTs 1 and 2 from the average of LVDTs 3 till 6.

Shear bolts in all specimens were preloaded, using direct torque

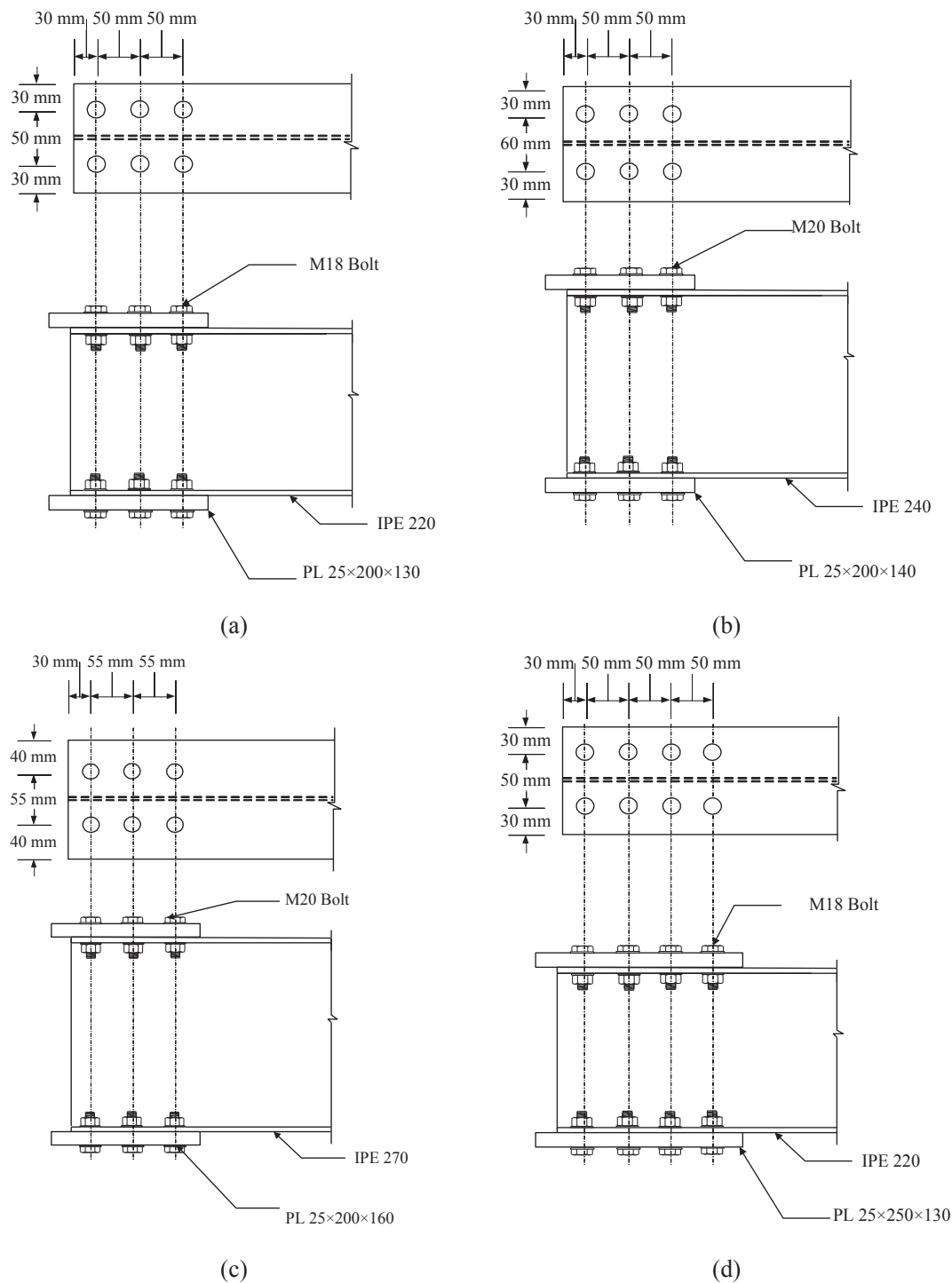


Fig. 2. Detailing of (a) MC1, (b) MC2, (c) MC3, and MC4.

Table 1
Tests results.

Section Name	Beam section	Bolts per row	Beam depth, d mm (in.)	Connection length, l mm (in.)	Ratio (l/d)	Failure mode	Failure load kN (kips)
MC1 (ST44)	IPE220	3	220 (8.66)	100 (3.94)	0.454	ABS	1141 (257)
MC2 (S355)	IPE240	3	240 (9.45)	100 (3.94)	0.416	ABS	1171 (263)
MC3 (ST44)	IPE270	3	270 (10.63)	110 (4.32)	0.407	ABS	1574 (254)
MC4 (ST44)	IPE220	4	220 (8.66)	150 (5.91)	0.681	NSF	1347 (303)

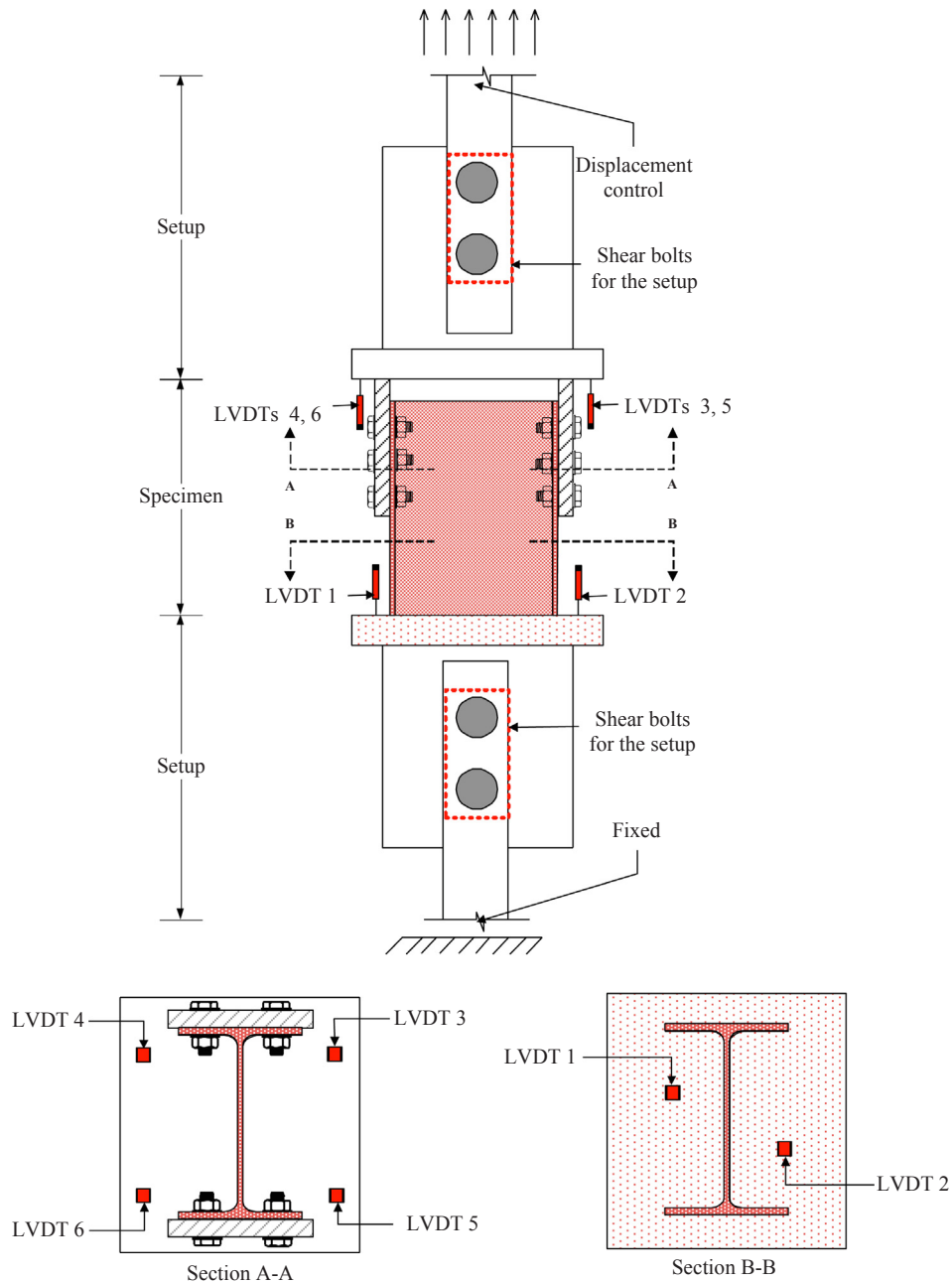


Fig. 3. Detailing of the setup and LVDT's distribution.

control, in accordance with the minimum pretension load available by the ANSI/AISC 360-16 [2].

The specimens were subjected to monotonic tensile loading ranging from 1 to 4 mm/min.

2.3. Experimental results

Two different failure modes occurred in the experimental program: ABS and NSF. Two limit states were reached prior to failure in all specimens: (1) shear bolts slip occurred at an early stage of the testing and (2) beam web local buckling occurred right after. Note that, the beam web local buckling was caused by a slight titling in the table of the testing machine. Also, note that it was observed in the experimental tests of structural Tees as well [5].

Table 1 summarizes the test results showing the failure mode, the ultimate load that the specimen sustained, and the connection length to beam depth ratio (L/d). This ratio was calculated by dividing the

connection length (total spacing between bolts) by the beam depth. Figs. 5 and 6 show the force-displacement response and the failure path of the specimens, respectively.

The results showed that specimens MC1, MC2, and MC3 failed by ABS in the beam section while specimen MC4 failed by NSF. Fig. 5 shows the load-displacement curves of all four specimens. Specimen MC3 has the largest cross section, hence the largest strength among all four specimens. The ultimate displacement of specimen MC3 (19 mm (0.75 in.)) was less than those of specimens MC1 and MC2 (≈ 26 mm (1.02 in.)) and slightly more than the ultimate displacement of specimen MC4 (18 mm (0.71 in.)). Also, the strain energy (indicated by the area under the force-displacement curve) consumed by the beam sections that failed by ABS is greater than the one consumed by the beam that failed by NSF.

Fig. 6(a) shows a close-up view of the ABS fracture path in MC3. It is observed that the failure starts by a full tensile fracture in the beam flange, followed by shear failure in the beam web toward the edge. Note

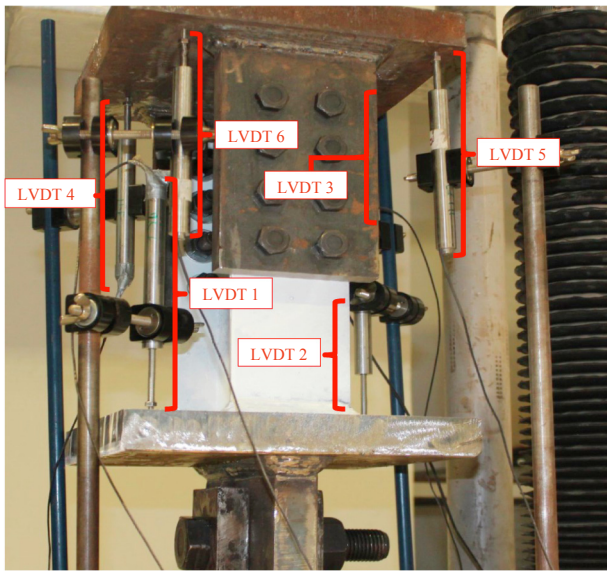


Fig. 4. LVDT's configuration.

that the observed shear failure combines both shear yielding and shear rupture which is consistent with the findings available in [6]. Fig. 6(b) shows the NSF fracture path in MC4. It is observed that the tensile fracture occurs along the entire beam section, propagating from the bottom beam flange toward the top beam flange. Both ABS and NSF

failure mechanisms start with a tensile rupture in the beam flange. Then, the yielding pattern in the beam web dictates the failure mode: ABS failure governs when the shear yielding path controls over the tensile rupture path in the beam web. Note that, the tests were terminated prior to full fracture of the beam flange and web to protect the setup holding the LVDTs. That is, Fig. 6 shows the failure path before full fracture of the beam flange and web.

The experimental results presented in Table 1 show that for beam depth of 220 mm (8.66 in.), ABS and NSF governed the behavior of MC1 and MC4, respectively. This indicates that for a constant beam depth, the failure mode changed from ABS to NSF by increasing the connection length (number of shear bolts). Also, the connection length to beam depth ratio (l/d) presented in Table 1 (column 6) shows that the ABS failure governed the behavior of the specimens having a low ratio (l/d). In fact, the beam depth ratio for specimens MC1, MC2, and MC3 was around 0.4 whereas the beam depth ratio for MC4 was around 0.7. Fig. 1(b) shows that ABS failure depends on two failure planes, the tensile fracture in the beam flange and the shear yielding and/or rupture in the beam web. The shear failure plane depends on the connection length and beam depth. As the connection length decreases, the shear failure plane becomes smaller. Thus, the ABS strength capacity becomes smaller and it controls the behavior of the connection. Similarly, the shear failure propagates throughout only a section of the beam web. When the beam depth increases, the NSF strength capacity becomes larger and the shear failure propagates to the nearest edge of the web. That is, the ABS failure controls over the NSF failure. It can be concluded that, as the beam depth increases and or the connection length decreases, the failure mode is controlled by ABS. Consequently,

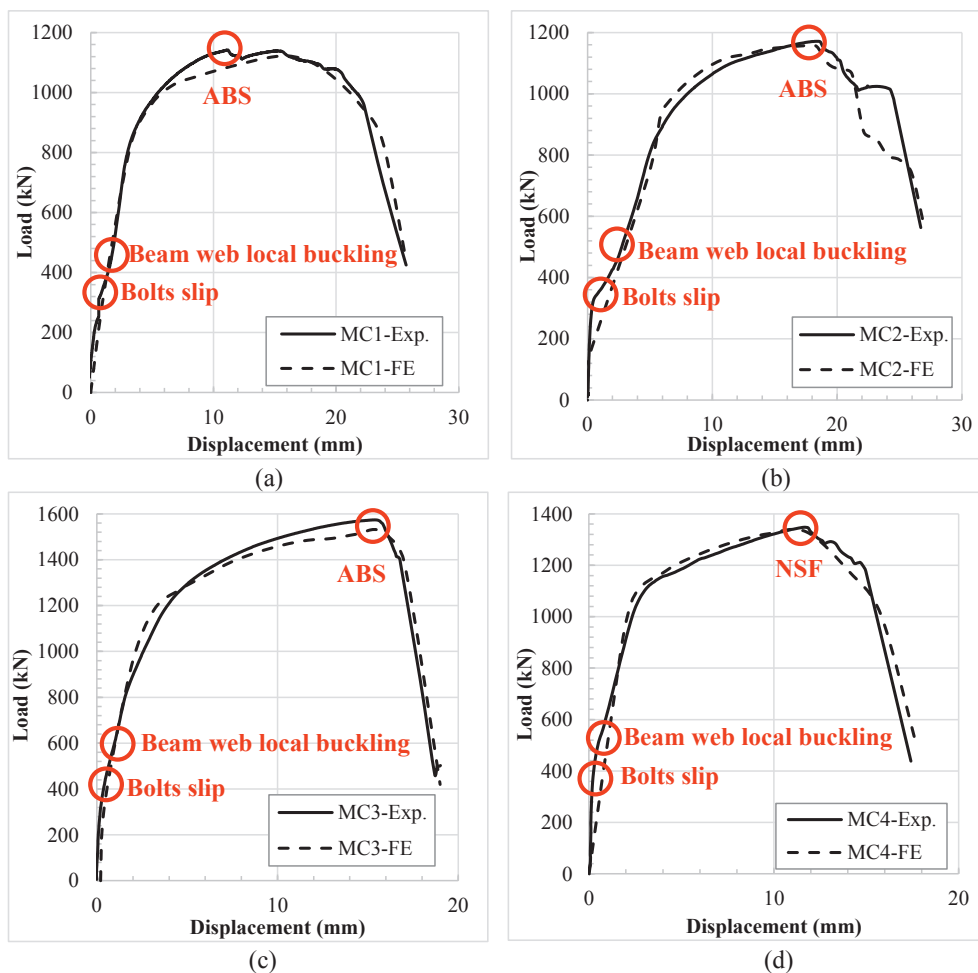


Fig. 5. Load-Displacement: experiment (Exp.) vs. FE fracture: (a) MC1, (b) MC2, (c) MC3, and MC4.

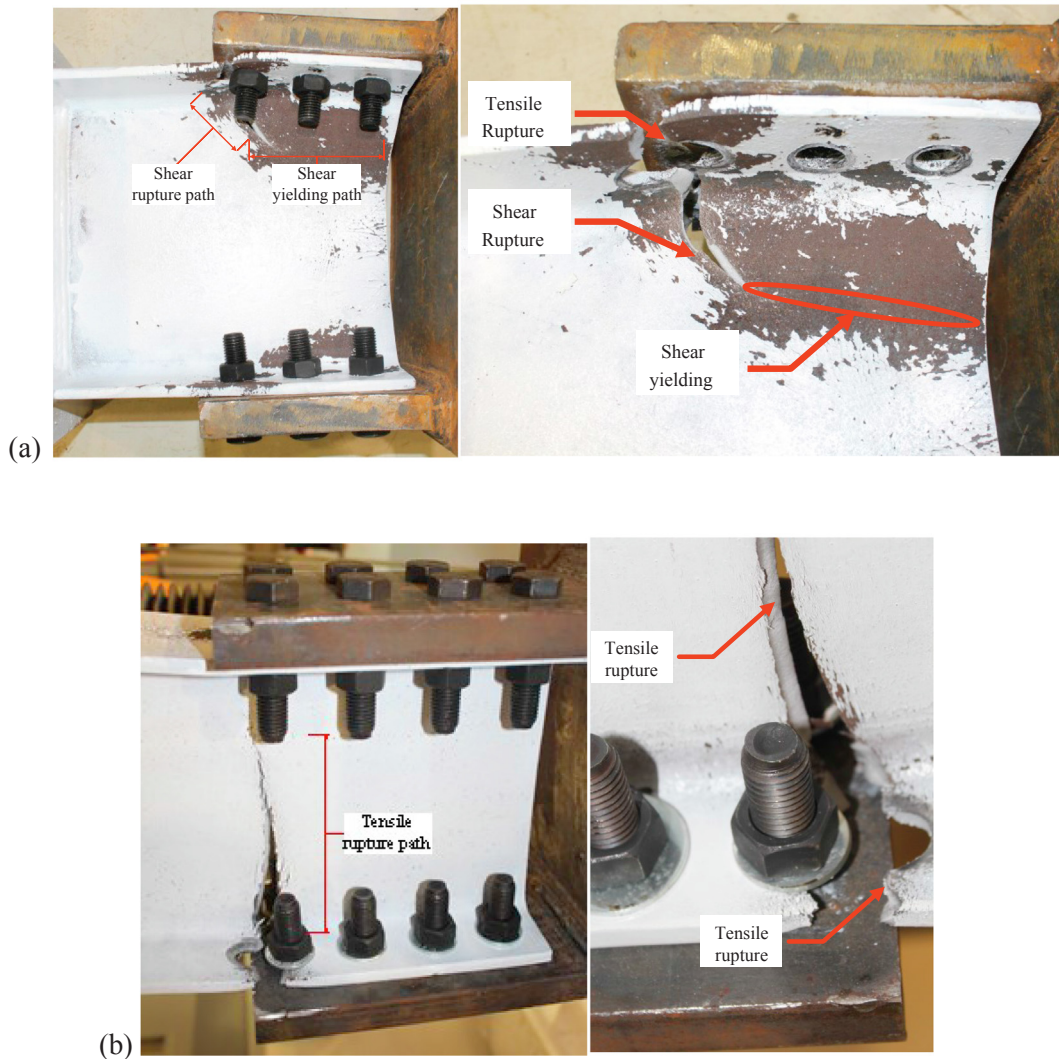


Fig. 6. Experimental failure path: (a) ABS in MC3 specimen and (b) NSF in MC4 specimen.

the beam depth and connection length are major parameters that impact the governing failure mode in beams of steel connections subjected to pure tensile loading. Also, ABS is a ductile failure mode.

Note that, the change in steel grade reported in Table 1, was due to lack of ST44 base material. The aim was not to study the steel grade effect on ABS failure. Specimen MC2 was added later to the testing batch and ST44 material was not available then. However, the response of specimen MC2 was as expected in terms of strength and failure mode. Furthermore, the analysis of the results was performed based on the connection length to beam depth ratio which is independent of the material used.

3. Existing strength models vs. experimental results

Another objective of this experimental research is to quantify the capability of the existing strength models to predict the ABS capacity in beams of steel connections. The experimental results conducted in this study were compared to the existing strength models developed by Epstein [3], and Driver et al. [6].

The strength model provided by Epstein [3] is:

$$R_n \leq \begin{cases} 0.6F_y A_{gv} + F_u A_{nt} & \text{(a)} \\ 0.6F_y A_{nv} + F_u A_{gt} & \text{(b)} \end{cases} \quad (1)$$

where A_{gv} is the beam gross shear area, A_{nv} is the beam net shear area,

A_{gt} is the beam gross tension area, A_{nt} is the beam net tension area, F_y is the steel yield stress, and F_u is the steel ultimate stress. Definitions of the tension and shear areas are available in [3].

The strength model developed by Driver et al. [6], also known as the *unified* equation is:

$$R_n = R_t A_{nt} F_u + R_v A_{gv} \left(\frac{F_y + F_u}{2\sqrt{3}} \right) \quad (2)$$

where R_t and R_v are the mean stress correction factors of the tension and shear areas, respectively. Their values can be found in [6].

The *unified* strength model considers that the rupture occurs in the net tension plane, and yielding and/or rupture occur in the shear plane. That is, the shear stress is taken as the average of shear yielding and shear rupture [6].

Table 2 shows the results of the comparison between the strength models and the experimental results. The mean test-to-predicted ratios of the *unified* strength model and Epstein strength model are 1.014 and 1.081, respectively. It can be seen that both strength models provided acceptable results, but the *unified* strength model had a mean test-to-predicted ratio closest to 1.0, and had the smallest coefficient of variation of 0.010. This indicates that the *unified* strength model better predicts the ABS capacity.

A comparison was made between the failure loads of ABS and block shear limit states. Table 2 shows the comparison between the ABS failure load (obtained from the strength models discussed earlier) and

Table 2
Test results vs. existing strength models (unified strength model and Epstein strength model) vs. block shear.

Specimen name	Test results	ABS Unified strength model [6]		ABS Epstein strength model [3]		Block shear equation [2] Capacity load kN (kips)	Test-to-block shear equation
		Capacity load kN (kips)	Test-to-predicted (T/P)	Capacity load kN (kips)	Test-to-predicted (T/P)		
Experimental tests	MC1	1141 (257)	1.021	1058 (238)	1.078	1241 (279)	0.92
	MC2	1171 (263)	1.020	1105 (249)	1.059	1214 (273)	0.96
	MC3	1574 (354)	1.002	1423 (320)	1.106	1673 (376)	0.94
	MC4	1347 (303)	1659 (373)	N/A	1521 (342)	N/A	2152 (484)

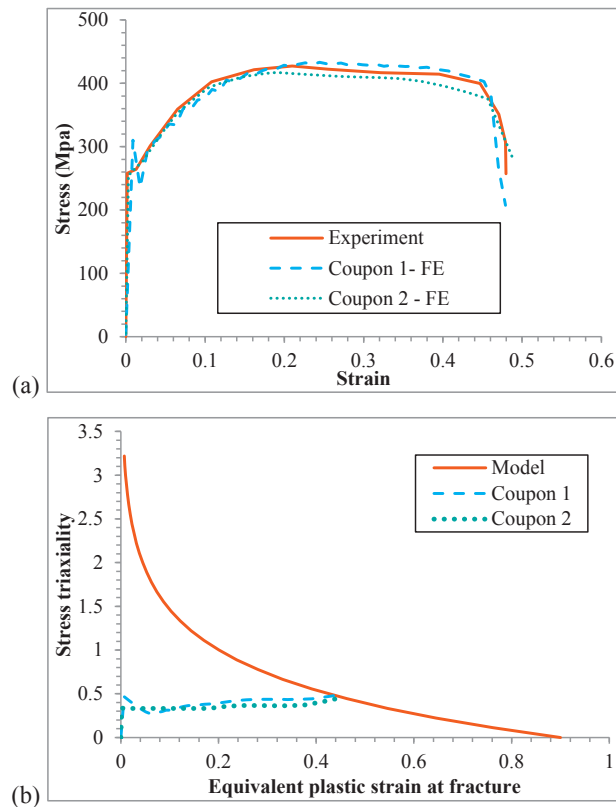
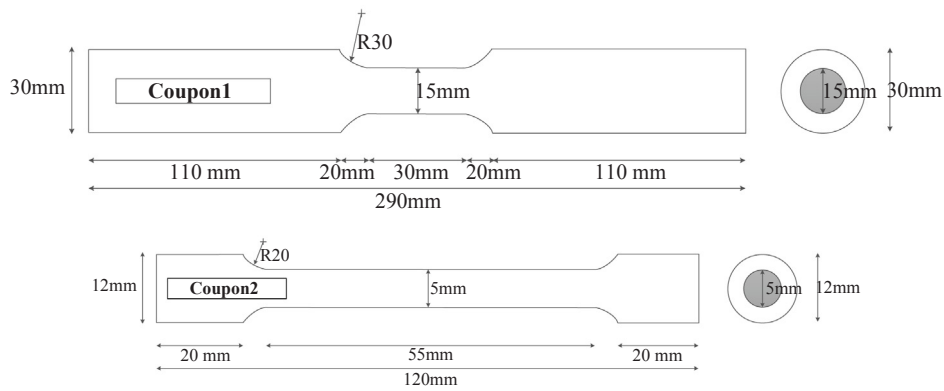


Fig. 7. ST44 steel material: (a) stress-strain, (b) stress triaxiality-equivalent plastic strain at fracture.

the block shear failure load (available in the ANSI/AISC 360-16 [2]). The results of the comparison clearly show that the ABS failure mode has a lower capacity than the block shear failure mode for both experimental results and strength models predictions of the tested connections. Also, the ratio of experimental results-to-“traditional” block shear strength indicates that for all tested specimens ABS governed over block shear since this ratio is less than 1. Thus including the ABS check

in current design codes for beams in steel connections subjected to pure tensile loading needs to be considered.

In conclusion, for the general case of I beam sections, ABS failure has one shear plane in the beam web compared to two shear planes in the beam flange for block shear failure. Recalling that the beam flange thickness is greater than the beam web thickness for the tested specimens, ABS governs over block shear. Thus, it is necessary to consider

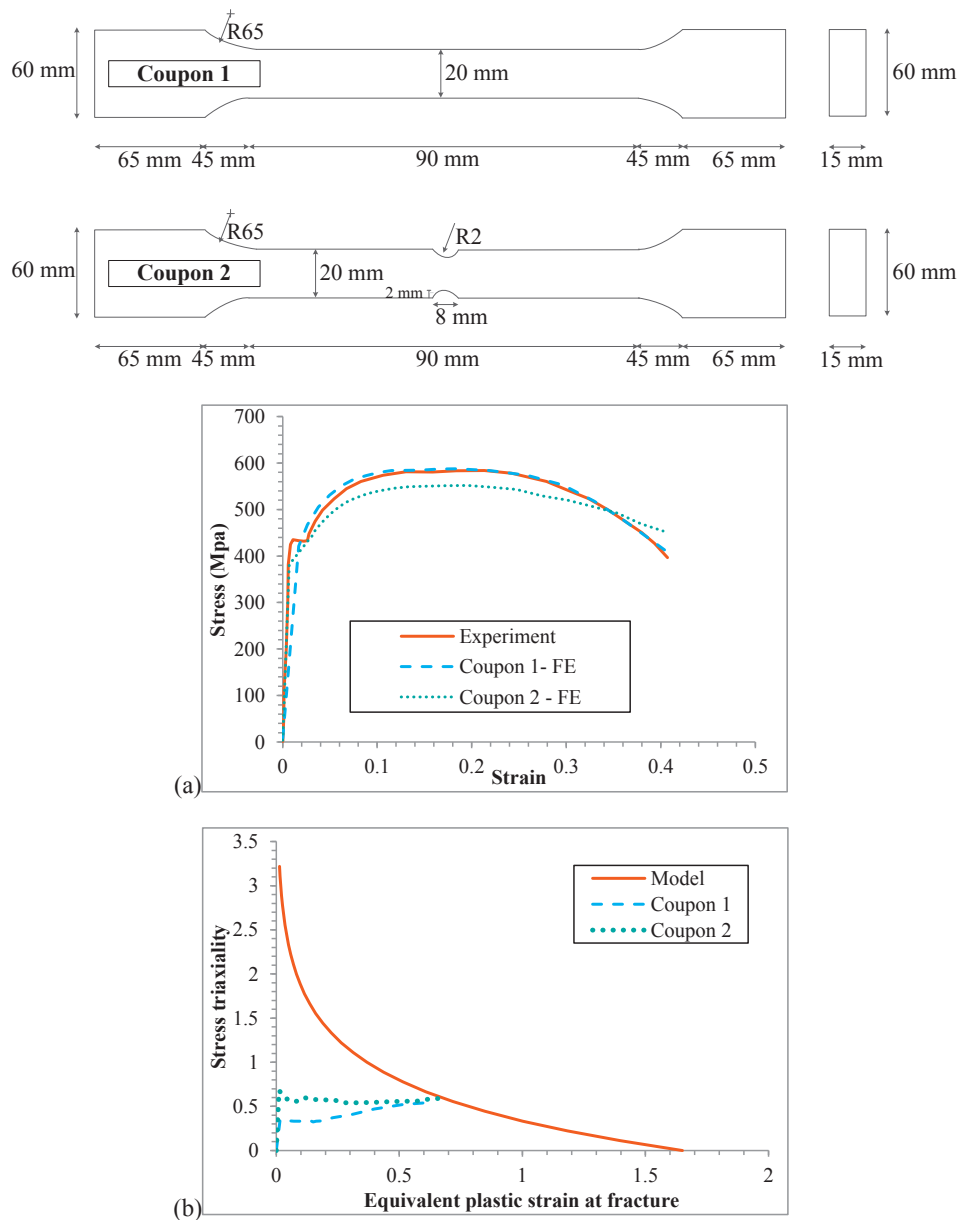


Fig. 8. S355 steel material: (a) stress-strain, (b) stress triaxiality-equivalent plastic strain at fracture.

ABS as a potential failure mode and include it in the current steel design codes as a design check.

4. FE fracture model

Three dimensional FE fracture models were developed to validate the experimental program performed as part of this research for the pre and post-yielding responses. Micromechanics fracture approach was used to model the ductile fracture of steel material in ABAQUS using predefined models. Ductile fracture is the sequential process of necking, micro-voids formation, coalescence of micro-voids to form a crack (crack grows 900 to applied stress), crack propagation by shear deformation, and fracture [8]. Several analytical and experimental models have been proposed to model ductile fracture of metals. The Rice and Tracey model [9], also known as Stress Modified Critical Strain model or SMCS, is used to model the ductile tension fracture of steel material and the Hooputra [10] model is used to model the ductile shear fracture of steel material. These models are predefined in ABAQUS. Both tension and shear fracture models were assigned for all steel material (ST44,

S355, and grade 10.9).

The Rice and Tracey model [9], known as “Ductile Damage” in ABAQUS, considers the void coalescence and propagation as the main processes that cause fracture to initiate. This tensile fracture model relates the strain at fracture in a material to the stress triaxiality as follows:

$$\varepsilon_p^f = \alpha \exp^{-\beta \eta} \quad (3)$$

where ε_p^f is the equivalent plastic strain at failure initiation due to tensile stresses, η is the stress triaxiality calculated as follows: $\eta = -\bar{\sigma} / \sigma_m$ where σ_m is the von Mises stress calculated as:

$$\sigma_m = \sqrt{\frac{(\sigma_1 - \sigma_2)^2 + (\sigma_1 - \sigma_3)^2 + (\sigma_2 - \sigma_3)^2}{2}} \quad (\sigma_1, \sigma_2, \sigma_3 \text{ are the principle stresses})$$

and $\bar{\sigma}$ is the hydrostatic or mean stress calculated as: $\bar{\sigma} = \frac{\sigma_1 + \sigma_2 + \sigma_3}{3}$. α is the toughness parameter indicating the material opposition to macro-voids formation and β is a material specific parameter related to modeling the process of void growth. This parameter was originally derived analytically by Rice and Tracey [9]. Despite many efforts to calibrate it for every material, recent research agreed on the statistical insignificance of the generated values of β .

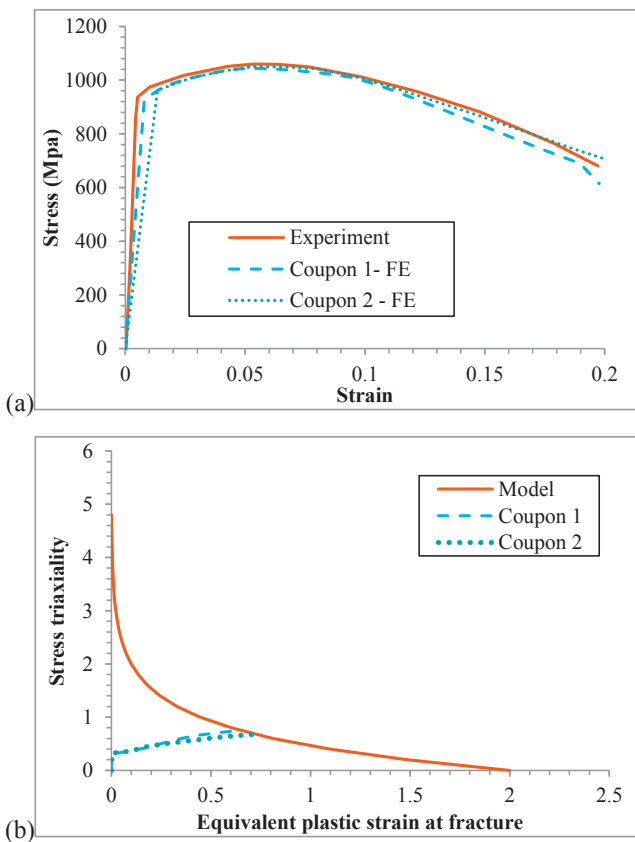
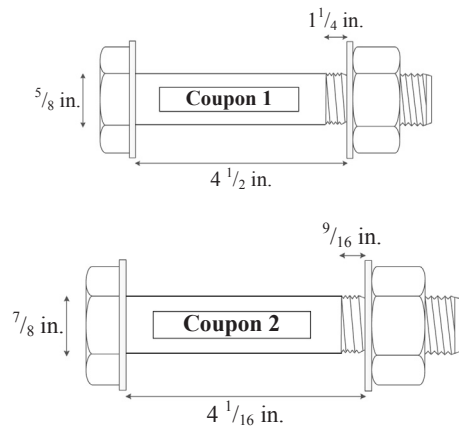


Fig. 9. Grade 10.9 steel material: (a) stress-strain, (b) stress triaxiality-equivalent plastic strain at fracture.

Table 3
Calibration of steel material.

Material	α	ϵ_s^+	ϵ_s^-
ST44 [16,17]	0.9	0.447	-1.487
S355 [18]	1.65	0.555	6.94
Grade 10.9 [19,20]	2	0.346	0.278

The model parameters, α and β , are specific for every material and need to be calibrated. The process of calibration was performed using trial and error on two geometrically distinct coupon tensile tests of every steel material. The coupons used to calibrate the steel material had different geometry (with/without notch) yielding different stress states for model calibration. Details of the calibration process and results are presented in the next section.

The *Hooputra* model [10] is used for the ductile shear fracture of the material. The following equation is defined:

$$\theta = \frac{1 - k_s \eta}{\phi} \quad (4)$$

where θ is the shear stress parameter, k_s is the material parameter in shear fracture curve, and ϕ is the ratio of maximum shear stress to von Mises stress.

The equivalent plastic strain at the onset of shear failure with respect to θ can be calculated as follows:

$$\epsilon_{p-s}^f = \frac{\epsilon_s^+ \sinh[f(\theta - \theta^-)] + \epsilon_s^- \sinh[f(\theta^+ - \theta)]}{\sinh[f(\theta^+ - \theta^-)]} \quad (5)$$

where ϵ_{p-s}^f is the equivalent plastic strain at failure initiation due to shear stresses, ϵ_s^+ & ϵ_s^- are the equivalent plastic strains in equibiaxial tension/compression at shear fracture respectively, f is a material parameter in shear fracture, and θ^+ & θ^- are shear stress parameters for equibiaxial tension/compression respectively, $\theta^+ = 2 - 4k_s$ and $\theta^- = 2 + 4k_s$.

Applying the *Hooputra* model [10], which is the one predefined in *ABAQUS* for ductile shear fracture, requires the user to calibrate several material parameters. Due to the lack of experimental results that are needed for the calibration process of the steel material, some parameters were obtained from the literature and others were calibrated.

Furthermore, both tensile and shear ductile fracture models depend on the damage evolution law represented by the damage variable, D . It is an index that describes the process of damage evolution starting from the first macro-crack formation where $D = 0$, till the fracture surface formation where $D = 1$. The damage evolution law can be specified in *ABAQUS* as fracture energy per unit area or plastic displacement at full failure [11]. In this research the plastic displacement approach was used. The plastic displacement at which full fracture occurs, u_f^{pl} , should be specified in *ABAQUS* and is related to the plastic strain at fracture, ϵ_f^{pl} , as follows: $u_f^{pl} = l^* \epsilon_f^{pl}$. The characteristic length, l^* , is determined through fractographic studies based on microstructural measurements such as grain size and dimple diameter. In this research a characteristic length (l^*) of 0.2 mm was used as recommended by Wang et al. [12].

4.1. Calibration of tension fracture

Rice and Tracey [9] derived analytically the value of β to be 1.5. Also, Myers et al. [13] showed that, despite being material dependent, a value of β of 1.5 is adequate for all steel material. As for the toughness parameter α , the process of material calibration consisted of reproducing the experimental results of two coupon tests (regular and notched coupons) for ST44, S355, and grade 10.9 using the true stress-strain characteristics of the material. The experimental results were first reproduced using an assumed value of α . The generated stress-strain curve was compared to the experimental one. The value of equivalent plastic strain and corresponding stress triaxiality at the center of the coupon at the necking point (location and instance of fracture initiation, respectively) were compared with the corresponding ones generated by the assumed value of α . The toughness parameter was varied until convergence of experimental and generated results. Note that, the stress triaxiality varies with the geometry of the coupon (regular vs. notched). That is, two geometrically distinct coupon tests were needed to validate the proposed toughness parameter for different values of stress triaxiality.

To calibrate the toughness parameter α , two coupons were simulated in the explicit solver FE analysis program *ABAQUS* including material nonlinearity. The weighted average method recommended by Ling [14] was used to simulate the true stress-strain curve of all steel material input. The engineering stress-strain characteristics used were obtained from the experimental results of coupon tests used in the calibration process. Besides material nonlinearity, geometric nonlinearity was considered in all analyses. The initial analysis included fracture

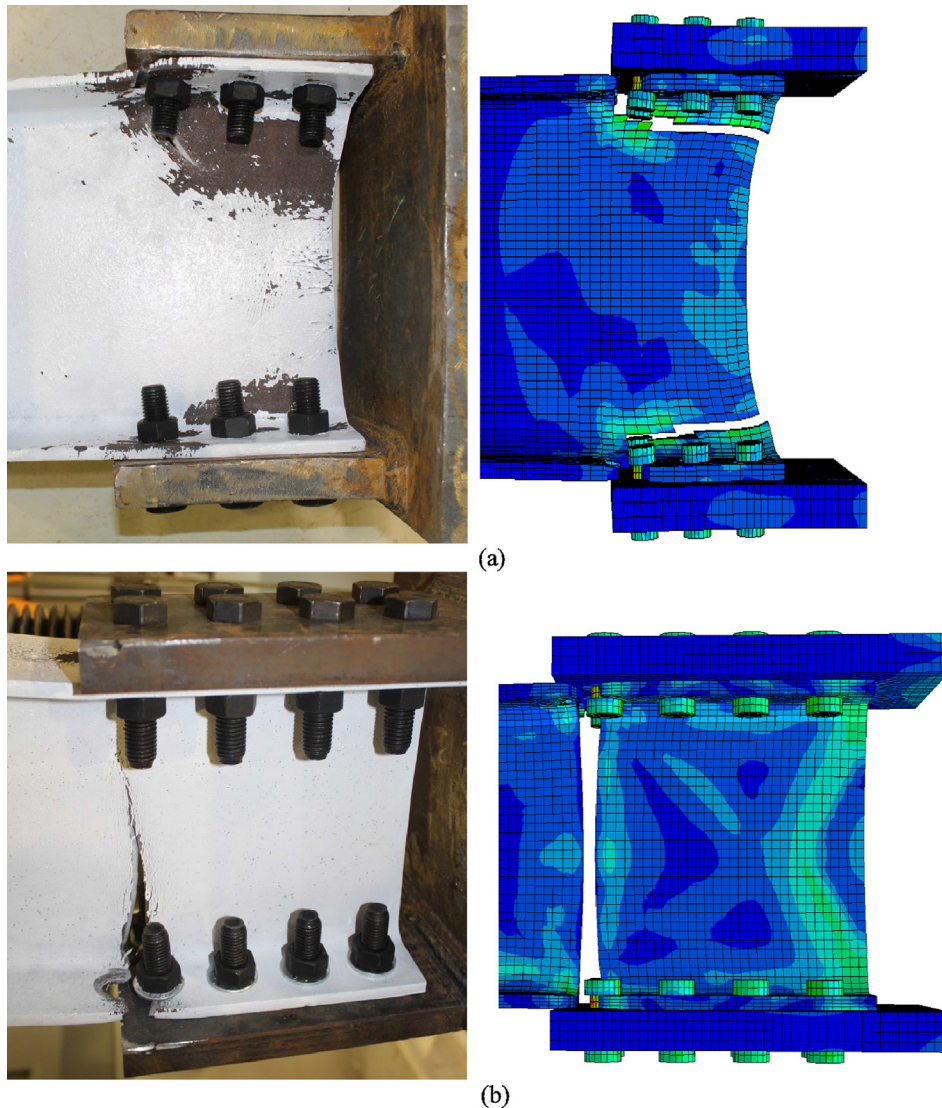


Fig. 10. Experiment vs. FE fracture paths: (a) ABS and (b) NSF.

simulation with an assumed toughness parameter of 2. Three-dimensional *C3D8R* solid brick elements were used. For the boundary and loading conditions, one end of the notched bar was fixed against rotation and displacement in all directions. The other end was released for displacement in the axial direction. Displacement was applied at the released end. To obtain the fracture toughness parameter, first the stress-strain curves of the simulated coupon tests were plotted against the experimental ones. Divergence between the two started at the necking point due to the assumed value of α . Second, the stress triaxiality versus strain at fracture history at the center of the coupon was plotted against the material specific curve generated using the assumed value of α , using Eq. (3). A process of trial and error was used to calibrate α for both stress-strain and stress triaxiality-strain at fracture for both coupons for every steel material. The results of the calibration (stress-strain and stress triaxiality-strain at fracture) of ST44 are shown in Fig. 7, those of S355 are shown in Fig. 8, and the ones of grade 10.9 are shown in Fig. 9. The calibrated values of α are presented in Table 3.

4.2. Calibration of shear fracture

Hooputra [10] developed the shear fracture model for aluminum alloys. The material parameter in shear fracture, f , was determined to

be 4.04 for quasi-static tests and 2.05 for dynamic tests for all metals. In this study f was taken 4.04. Moreover, Adewole and Teh [15] determined k_s to be 0.1 for steel material. Subsequently, $\theta^+ = 1.6$ and $\theta^- = 2.4$.

For the calibration of ε_s^+ and ε_s^- , the coupons used for tension calibration were used also to calibrate the shear fracture parameters. At the boundaries of the notched region, fracture is caused by shear stresses, thus, the shear stress parameter, θ , was calculated from the stress results at the boundaries of the fractured area. Also, the equivalent plastic strain at shear fracture ε_{p-s}^f was obtained from the FE output results at the boundaries of the notch. For every steel material, ε_s^+ and ε_s^- were obtained by solving Eq. (5) for the two coupons. The results of the shear fracture parameters calibration are also presented in Table 3.

5. Numerical results

The FE models were developed in *ABAQUS* to reproduce the load-deformation response and fracture paths of the experimental program performed as part of this research.

5.1. Geometric, force boundary, and material properties

The four tested specimens were reproduced in *ABAQUS*. The

specimens were loaded in two steps. In the first step, bolts were pre-tensioned by applying a pressure equivalent to the minimum required pretension force. In the second step, a displacement controlled monotonic load was applied at the tip of the setup plates. During all steps of the analysis, the edge of the beam was fixed. The complete true stress-strain curve was used for all steel materials with isotropic hardening. Both tension and shear fracture models were specified for all steel material regardless of the expected failure mode. Thus, the failure envelopes were automatically tested at every load increment and the governing one defined the failure pattern.

5.2. Model discretization

Discretization of all the components of the connection model in *ABAQUS* was performed using explicit *C3D8-R* (eight-node brick elements with reduced integration). At regions where failure was expected to occur and at regions where stress was likely to concentrate (around bolt holes) a finer and a mapped mesh were adopted in order to advance the accuracy of interpolations. Surface-to-surface contact with a finite sliding coefficient was used to reproduce contact surfaces between all components of the specimens. This finite sliding was used to represent a friction coefficient of 0.25. The finite sliding allowed separation, sliding, and rotation of the contact surfaces. A general contact interaction was specified to overcome the excessive distortion issues faced in the explicit fracture modeling. Finally, the *STATUS* field output was activated for the fracture to be visualized.

5.3. Comparison of FE predictions with experiments

The capability of the FE fracture model to predict the fracture response of beams in steel connections subjected to pure tensile loading was validated against the four tests conducted as part of this research. The load-deformation curves of all specimens are shown in Fig. 5. It can be seen that for all specimens, the FE results predicted well the initial stiffness and both the yield and ultimate loads. In addition, the developed FE fracture models were able to predict the post-ultimate deformation of beams failing in ABS and NSF. Fig. 10 shows a comparison of the failure paths of both ABS and NSF limit states between the FE fracture results and the experimental results. It is shown that the FE fracture path was similar to the experimental one. For ABS, the tension fracture in the beam flange was followed by shear yielding and fracture in the beam web. For NSF, pure tension fracture developed in the beam section. The FE fracture models predicted well the connection response when compared to experimental results. Thus, the developed FE fracture models can be used in future numerical parametric studies to investigate further the ABS failure mode.

6. Conclusions

In designing steel connections all failure modes are needed to be accounted for including the ABS failure. In fact, when large tensile demands are developed in steel connections, ABS becomes a potential failure mode. That is, ABS failure might occur in the beam section. Experimental and analytical investigations were performed to investigate further the ABS failure. Experimental results showed that two different failure modes (ABS and NSF) governed the behavior of the connections depending on the beam depth and connection length. Furthermore, the results showed that as the beam depth increases and/or the connection length decreases the failure mode is controlled by ABS. Also, existing strength models were tested against the experimental results conducted as part of this study. As a result, the *unified* strength model showed excellent agreement with the experimental results and was recommended to be used in predicting the ABS capacity load. A comparison between ABS and block shear capacities showed that ABS is more critical for the tested connections. Thus, it is essential to include it in the current design check of steel structures. Also, the

experimental results showed that ABS is a combination of both yielding and rupture and can be considered a ductile failure mode. Although ABS might not be the governing failure mode, it can potentially be the next failure mode to occur. That is, predicting the response after first component yielding is necessary. Thus, FE fracture models were developed to predict both pre-yielding and post-yielding responses of the ABS failure mode. Tension and shear ductile fracture models were calibrated for base and bolt steel material. Then, the fracture parameters were implemented in *ABAQUS* to reproduce the experimental results. The developed FE fracture models were validated against experimental results and showed excellent prediction of the load-displacement curves and failure paths and modes in all four specimens. Finally, the performed experimental and analytical investigations are part of an ongoing research that aims at including the ABS failure mode in the current steel design codes to ensure a safe design. Full scale experimental tests of moment connections associated with deep beam sections will be the subject of future research to characterize ABS in these connections. Also, the developed FE fracture models are to be used in future parametric studies to further characterize the ABS failure mode in full scale connections.

Acknowledgments

The authors gratefully acknowledge the financial support provided by the American University of Beirut Research Board under grant No. 103604-24705. Also, the corresponding author would like to thank the National Council for Scientific Research in Lebanon and the American University of Beirut, CNRS-L/AUB, PhD award program 2017–2018 for the support of the PhD student.

References

- [1] Prequalified connections for special and intermediate steel moment frames for seismic applications-ANSI/AISC 358-16. Chicago, US; 2016.
- [2] An American National Standard. Specification for structural steel buildings-ANSI/AISC 360-16, Chicago, US; 2016.
- [3] Epsein H. Block shear of structural tees in tension - alternate paths. *Eng J* 1996;33(4):147–52.
- [4] Epstein H, McGinnis M. Finite element modeling of block shear in structural tees. *Comput Struct* 2000;77(5):571–82.
- [5] Epstein H, Stemberg H. Block shear and net section capacities of structural tees in tension: test results and code implications. *Eng J* 2002;Fourth Quarter:228–39.
- [6] Driver RG, Grondin GY, Kulak GL. Unified block shear equation for achieving consistent reliability. *J Constr Steel Res* 2006;62:210–22.
- [7] Cai Q, Driver RG. Prediction of bolted connection capacity for block shear failure along atypical paths. *Eng J* 2010:213–21.
- [8] Chi W, Kanvinde A, Deierlein G. Prediction of ductile fracture in steel connections using SMCS criterion. *J Struct Eng* 2006;132(2):171–81.
- [9] Rice J, Tracey D. On the enlargement of voids in triaxial stress fields. *J Mech Phys Solids* 1969;17(3):201–17.
- [10] Hooputra H, Gese H, Dell H, Werner H. A comprehensive failure model for crashworthiness simulation of aluminum extrusions. *Int J Crashworthiness* 2004;9(5):449–64.
- [11] Lecture 9: material damage and failure. *ABAQUS/explicit: advanced topics*; 2005.
- [12] Wang Y, Zhou H, Shi Y, Xio J. Fracture prediction of welded steel connections using traditional fracture mechanics and calibrated micromechanics based models. *Int J Steel Struct* 2011;11(3):351–66.
- [13] Myers A, Kanvinde A, Deierlein G. Calibration of the SMCS criterion for ductile fracture in steels: specimen size dependence and parameter assessment. *J Eng Mech* 2010;136(11):1401–10.
- [14] Ling Y. Uniaxial true stress-strain after necking. *AMP J Technol* 1996;5:37–48.
- [15] Adewole K, Teh L. Predicting steel tensile responses and fracture using the phenomenological ductile shear fracture model. *J Mater Civ Eng* 2017;29(12):06017019.
- [16] Versailot P. Effect of cyclic loading on the mechanical properties of steel PhD dissertation Romania: Universitatea Politehnica Timisoara; 2015.
- [17] Brnic J, Turkalj G, Vukelic G. Importance of experimental research in the design of structures. *Annals of DAAAM for 2012 & proceedings of the 23rd international DAAAM symposium*. 2012.
- [18] Ribeiro J, Santiago A, Rigueiro C. Damage model calibration and application for S355. 21st European conference on fracture-ECF21, Catania, Italy, EU. 2016.
- [19] Moore A, Rassati G, Swanson J. Evaluation of the current resistance factors for high-strength bolts. *Research Council on Structural Connections*; 2008.
- [20] Christopher R. Calibration of alloy steel bolts Master's thesis Lehigh University; 1964.